Wall Pressure Signature in Compressible Turbulent Boundary Layers

N.A. Buchmann, Y.C. Kücükosman, K. Ehrenfried and C.J. Kähler

Abstract Large-scale turbulent flow structures associated with positive and negative wall pressure fluctuations in a compressible turbulent boundary layer are investigated. Experiments are conducted in a closed-loop transonic wind tunnel at Ma = 0.5–0.8, $\mathrm{Re}_\tau = 5{,}100$–$9{,}500$ with combined velocity field and wall pressure measurements. Both, velocity and pressure statistics are analysed and compare well with existing low Mach number data. Spatial two-point correlation is applied to determine the size and orientation of the large-scale flow structures, which depending on the wall height have an averaged length scales of 4–6 δ and a maximum inclination angel of $\approx$12°–13°. The wall pressure fluctuations are associated with shear layer structures and it is shown that positive pressure fluctuations are correlated with low speed large-scale flow structures over streamwise extents of 4–5 δ.

1 Introduction

Understanding the relationship between coherent flow structures and associated wall pressure fluctuations in turbulent boundary layers is fundamental in the prediction and control of wall-bounded turbulent flows. In incompressible flows the turbulent velocity field and the fluctuating pressure field are connected by the solution of the Poisson's equation [10].

$$\nabla^2 p = -\rho\, \tilde{u}_{i,j} \tilde{u}_{j,i}, \tag{1}$$

where ρ is the fluid density and $\tilde{u}_{i,j}$ the partial derivative of the velocity $\tilde{u}_i = U_i + u_i$. Assuming the boundary layer flow is two-dimensional and homogenous in spanwise and streamwise direction Eq. 1 simplifies to

N.A. Buchmann (✉) · Y.C. Kücükosman · C.J. Kähler
Institute of Fluid Mechanics and Aerodynamics, Bundeswehr University Munich, 85577 Neubiberg, Germany
e-mail: nicolas.buchmann@unibw.de

K. Ehrenfried
Institut Für Aerodynamics and Fluid Mechanics, German Aerospace Center (DLR), 37073 Göttingen, Germany

M. Stanislas et al. (eds.), *Progress in Wall Turbulence 2*,
ERCOFTAC Series 23, DOI 10.1007/978-3-319-20388-1_8

$$\frac{1}{\rho}\nabla^2 p = -2\frac{dU}{dy}\frac{u_2}{dx} - u_{i,j}u_{j,i}. \tag{2}$$

The two terms on the right hand side represents the pressure sources. The first term is frequently referred to as the fast, or linear *mean−turbulent* pressure source and the second slow, nonlinear $turbulent–turbulent$ interaction.

According to Farabee and Casarella [4] wall pressure fluctuations can be classified as low and high frequency fluctuations, which originate in the inner and outer region of the boundary layer. Significant contribution to the high wavenumber fluctuations comes from the viscous sublayer, while the logarithmic layer largely contributes to low wavenumber fluctuations [2]. Of particular interest are high-amplitude pressure peaks (HAPPs) with strong fluctuations 2–3 times above the r.m.s. pressure fluctuations. These pressure events have a low occurrence probability, but large contribution to the total r.m.s. pressure [11]. It is believed that positive pressure fluctuations are associated with shear layer structures and sweep–ejection events [13], while large negative pressure fluctuations are related to spanwise and quasi-streamwise vortices [6].

The wall pressure is affected by the entire velocity field as given by (2) and the role of large-scale flow structures, originating in the logarithmic and outer layer (i.e. super-structures,VLSM), in this relationship is yet nuclear. Large-scale flow structures are characterised by long meandering regions of positive and negative velocity fluctuations with significant contribution to the overall Reynolds stress [8]. More importantly, the large-scale flow structures have a direct influence on the near-wall cycle via amplitude modulation of the small-scale velocity fluctuations [9].

By logic extension one can hypothesis a similar connection between the large-scale structures and the fluctuating wall pressure field. Therefore, the present study applies simultaneous velocity and wall pressure measurements to first identify the large-scale flow structures and second to link them to the fluctuation wall pressure field.

2 Experimental Procedure

2.1 Turbulent Boundary Layer Experiment

Experiments are conducted in the Transonic-Wind-Tunnel at DLR Göttingen (TWG). The TWG can be operated continuously and has a 4.5 m long adaptive test section with 1×1 m^2 cross-sectional area. The wind tunnel and plenum chamber are pressurised such that the Mach number Ma and stagnation pressure p_0 can be adjusted independently. A rigid plate of 2.75 m length and 1 m span is mounted symmetrically in the test section (Fig. 1). The plate has an elliptical nose and the flow is tripped 180 mm downstream of the leading edge. Adaption of the upper and lower test section wall ensures a nearly nearly zero pressure gradient, which decreases slightly towards

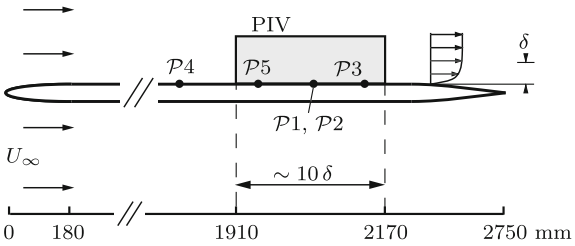

Fig. 1 Side view of the experimental setup showing with the boundary layer plate, pressure transducers $\mathcal{P}1-5$ and PIV measurement region

Table 1 Characteristics of the turbulent boundary layer for the different operating conditions (Ma, p_0) considered in the present study

Ma	p_0 (kPa)	U (m/s)	u_τ (m/s)	δ (mm)	θ (mm)	ν/u_τ (μm)	Re_τ	Re_θ
0.5	50	173.9	6.00	26.8	4.0	5.3	5,100	16,700
0.8	50	274.8	9.32	26.5	3.7	3.4	7,800	24,800
0.5	100	178.4	5.90	26.8	3.7	2.8	9,500	31,200

the end of the plate. The wind tunnel is operated at free-stream Mach numbers Ma = 0.5 and 0.8 and stagnation pressures $p_0 = 50$ and 100 kPa. Under these conditions the Reynolds number is $\mathrm{Re}_\tau = 5{,}100$–$9{,}500$ and the boundary layer thickness is $\delta = 26$–27 mm (see Table 1).

2.2 Velocity Field and Wall Pressure Measurements

In order to resolve the large and very large scale flow structures simultaneous planar PIV measurements with three sCMOS cameras are conducted to cover a large streamwise field-of-view of $1.5 \times 10\ \delta$. The cameras have a sensor size of 2560×2160 pixel^2 and 6.5 μm pixel pitch and are equipped with 100 mm focal length Zeiss macro lenses with an optical magnification of $\mathcal{M} = 0.17$. Illumination in the $x-y-$plane is provided by a Spectra Physics Quanta-Ray PIV 400 Nd:YAG dual-cavity laser. The light-sheet with a thickness of 0.5–1 mm thickness is introduced from the trailing edge of the flat plate model. The flow is seeded with DEHS droplets with 1 μm mean diameter. A total of 20,000 images are recorded and analysed with an iterative multi pass window-correlation routine. The final interrogation window size is 16×16 pixel^2 with 50 % overlap. This corresponds to a spatial resolution of 0.62 mm or $\Delta x^+ = 116 - 489$ depending on Re_τ.

The measurement section is equipped with 9 static pressure taps and an array of 5 dynamic piezo-resistive pressure transducers (EPE-S449-0.35B, Entran) (see [3] for details). Transducers $\mathcal{P}3-\mathcal{P}5$ are aligned with the light-sheet in streamwise direction and have a mean separation of approximately 7.5δ (see Fig. 1). Transducer $\mathcal{P}1-\mathcal{P}2$

are located of-axis at identical streamwise positions and spanwise separation of 0.23 δ and are used to assess the spanwise coherence of the pressure fluctuations across the light-sheet width. The pressure transducers have a sensing diameter of 2.4 mm and a 35 kPa pressure range. In order to improve the spatial resolution the sensors are mounted in an adaptor and connected to the surface pressure via a 0.5 mm orifice. Thus, depending on Re_τ the effective spatial resolution of the dynamic pressure measurements is $d^+ = du_\tau/\nu = 94$–147. Note that in order to fully resolve the wavenumber spectrum of the pressure fluctuations a resolution of $d^+ \leq 10$–12 is required [7, 11]. Consequently, the present measurements are restricted to large-scale pressure fluctuations only. A static calibration is performed for each transducer and the analog pressure signals are pre-amplified via a Endevco signal conditioner. The AC component of the signals are filtered and digitised by a Dewetron A/D converter at a rate of 20 kHz ($\Delta t u_\tau^2/\nu = 137$) over a time period of 500 s ($TU_\infty/\delta > 10^6$). In addition the camera and Q-switch trigger signal are also digitised such that the velocity and dynamic wall pressure measurements can be synchronised off-line.

3 Characterisation of the Turbulent Boundary Layer

3.1 Velocity Field Statistics

An example of the instantaneous velocity field at $\mathrm{Ma} = 0.8$, $\mathrm{Re}_\tau = 7{,}800$ is given in Fig. 2. The velocity field consists of a hierarchy of coherent δ-scale structures that appear to be inclined in the streamwise direction by approximately 14°. The intermittency of the turbulent/non-turbulent interface is also clearly visible. The turbulent boundary layer develops in streamwise direction and δ and Re_τ increase by approximately 8 % over a distance of 10 δ. Mean flow statistic sampled in the center of the domain are summarised in Table 1 for the two Mach numbers investigated in this study. Mean velocity and Reynolds normal stress profiles are illustrated in Fig. 3 and are in good agreement with the data of Fernholz and Finley [5]. Since the focus of the current study is on the large-scale flow structure the measurements only resolve the flow in the logarithmic region and the outer part of the turbulent boundary layer (i.e. $800 \leq y^+ \leq 1.5\delta^+$).

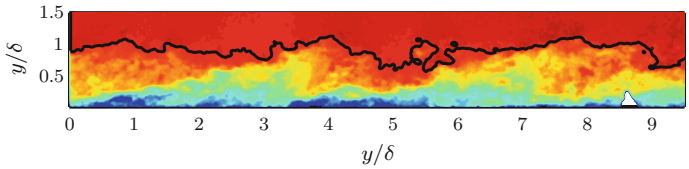

Fig. 2 Instantaneous velocity field U/U_∞ for $\mathrm{Re}_\tau = 7{,}800$ ($\mathrm{Ma} = 0.8$). *Black line* indicates the boundary layer thickness δ and colour contours are from 0.5 to 1.0

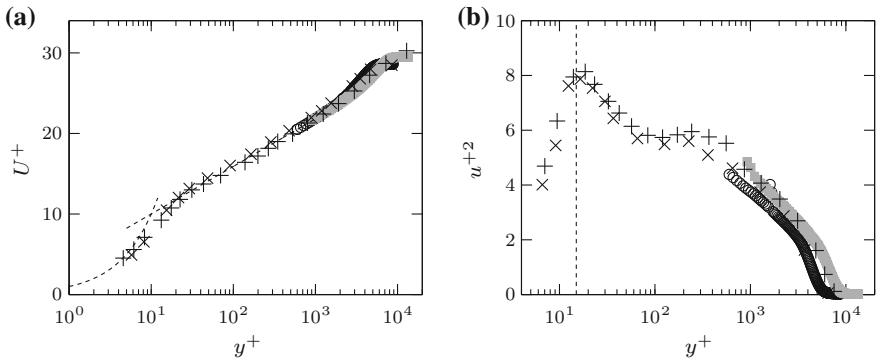

Fig. 3 Mean velocity profile U^+ (**a**) and Reynolds normal stress u^{+2} (**b**) in inner scaling. Present data: ∘, $\mathrm{Re}_\tau = 5{,}100$ (Ma = 0.5); ■, $\mathrm{Re}_\tau = 7{,}800$ (Ma = 0.8); ×,+, Fernholz and Finley [5]

3.2 Statistical Properties of Wall Pressure Fluctuations

Typical power density spectra of the wall pressure fluctuations Φ_{pp} for sensor $\mathcal{P}1-\mathcal{P}4$ are shown in Fig. 4. The spectra show distinct peaks at the low frequency range, which are associated with tones produces by the wind tunnel turbine and structural vibrations of the test section. These acoustic fluctuations decay rapidly at higher frequencies and the power spectrum becomes dominated by the convective pressure fluctuations for frequencies above 1.5–2 kHz [3]. In the range from 2 to 10 kHz the spectra are flat and do not show a maximum typically seen in low Mach number boundary layers. The cut-off frequency of the Helmholz resonator is approximately 11 kHz above which the pressure fluctuations are attenuated by more than −3 dB (see [3] for details). In order to remove the acoustic pressure fluctuations the

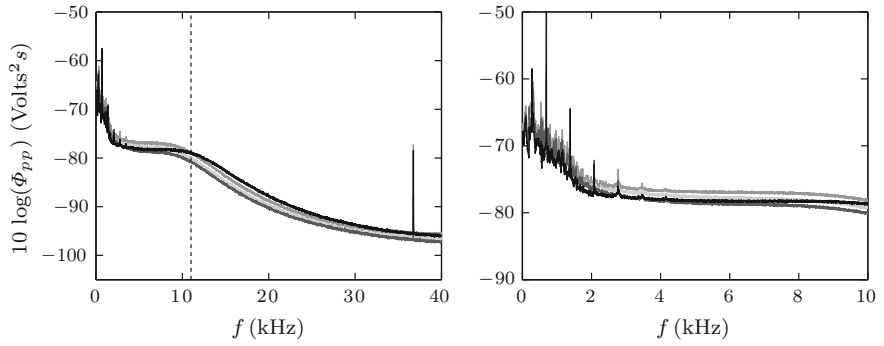

Fig. 4 Power spectral density of the wall pressure fluctuations Φ_{pp} for $\mathrm{Re}_\tau = 7{,}800$ (Ma = 0.8) and sensors: —— $\mathcal{P}1$; —— $\mathcal{P}2$; —— $\mathcal{P}3$; —— $\mathcal{P}4$. The *dashed line* indicates the −3 dB cut-off frequency of the Helmholz resonator

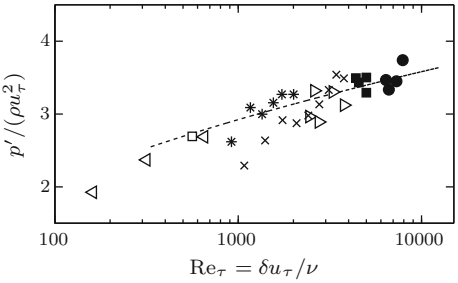

Fig. 5 Root-mean-square wall pressure p' in inner scaling as a function of the Reynolds number. Present results: ■, $\mathrm{Re}_\tau = 5{,}100$ (Ma = 0.5); •, $\mathrm{Re}_\tau = 7{,}800$ (Ma = 0.8). ▷, Bull and Thomas [1]; ∗, Farabee and Casarella [4]; □, Schewe [11]; ×, Tsuji et al. [14]; ◁, Spalart [12]; – – – – $(p'/\rho u_\tau^2)^2 = 6.5 + 1.86\ln(\mathrm{Re}_\tau/333)$ [4]

signals are filtered at 1.5 kHz using a phase preserving high-pass filter. The filter frequency is optimised by comparing the pressure auto-correlations, which remain largely unchanged for filter frequencies above 1.5 kHz.

The r.m.s. values of the filtered wall pressure fluctuations p' normalised by inner scaling are plotted in Fig. 5 together with previous results. The r.m.s. wall pressure increases slowly with Re_τ and follows the prediction $(p'/\rho u_\tau^2)^2 = 6.5 + 1.86\ln(\mathrm{Re}_\tau/333)$ of Farabee and Casarella [4]. The current result for Ma = 0.5 and Ma = 0.8 also follow this trend and extend the currently available data to larger Re_τ.

The probability density function (PDF) of the wall pressure fluctuations is shown in Fig. 6. The PDFs are normalised by p' and displayed in linear and logarithmic scaling. The PDFs show little variation with Mach number, respectively Reynolds number

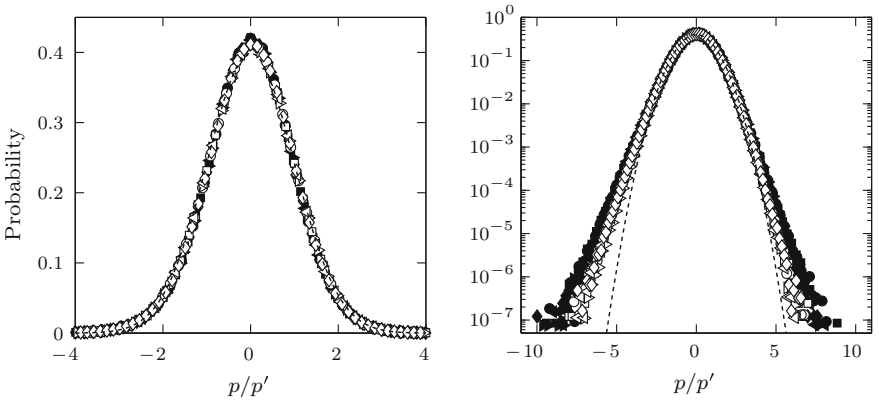

Fig. 6 Probability density function of wall pressure fluctuations. Symbols indicate the different sensors $\mathcal{P}1-\mathcal{P}5$. *Solid symbols*, $\mathrm{Re}_\tau = 5{,}100$ (Ma = 0.5); *open symbols*, $\mathrm{Re}_\tau = 7{,}800$ (Ma = 0.8); ·····, Gaussian distribution

and obey a near Gaussian distribution. However, the tails of the PDFs approach an exponential distribution and show some slight dependency on the Reynolds/Mach number, which agrees well with observations in [14]. The skewness is approximately -0.09 for both cases and consistent with the low Mach number data of Gravante et al. [7]. The flatness decreases from 3.6 to 3.3 with increasing Re_τ and also follows the trends in [7] albeit at different spatial resolutions. It is important to note that spectral quantities and higher order statistics are dependent on the spatial resolution as pointed out in [7, 11] and that some caution needs to be taken when interpreting data from different sources.

4 Organisation of the Large-Scale Flow Structures

Two-point velocity correlations of the form $R_{uu}(\xi, y) = \langle u(x-\xi, y_p)\, u(x, y) \rangle$ for the Ma = 0.8 ($\mathrm{Re}_\tau = 7{,}800$) case and different wall heights of the conditioning point y_p are shown in Fig. 7. The averaged coherent flow structures extend over large streamwise domains (5–6 δ) and have large wall-normal extends (0.75–1 δ). The structures maintain their coherence for different wall height, but their streamwise length scale decreases with wall height (Fig. 8a). Different Mach/Reynolds numbers exhibits a good collapse when scaled on outer variables similar to the low Mach number data in Hutchins and Marusic (2007) [8]. Although the present data indicate averaged streamwise length-scales that are approximately 25–50 % larger than those given in [8] (see Fig. 9a). The contours of R_{uu} show a clear inclination in streamwise direction, which increase from approximately 3° near the wall ($y/\delta = 0.1$) to a maximum angle of 12°–13° at $y/\delta - 0.5$. The regions of positive correlations reach far into the boundary layer and persist over large streamwise extents and give an indication of the average size of the superstructures or VLSM-type events in the outer region of the turbulent boundary layer.

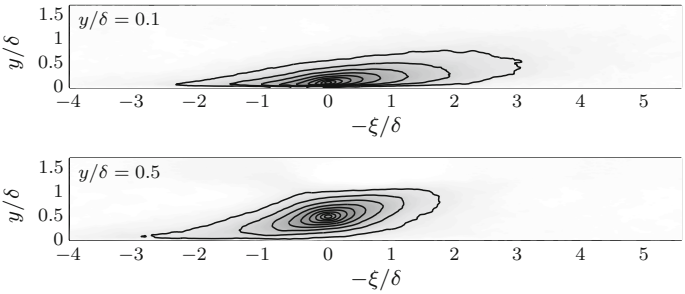

Fig. 7 Two-point correlation of the streamwise velocity fluctuation $R_{uu}(\xi, y)$ for $\mathrm{Re}_\tau = 7{,}800$ (Ma = 0.8) calculated at $y/\delta = 0.1$ (*top*) and $y/\delta = 0.5$ (*bottom*). Contour levels are from $R_{uu}/u'^2 = 0.1$ to 1.0 in increments of 0.1

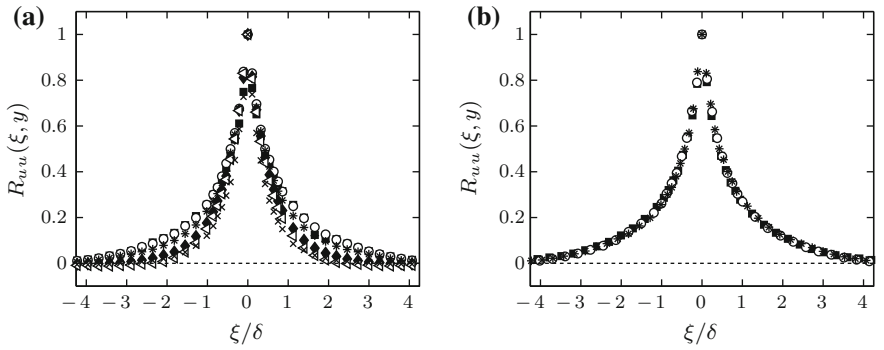

Fig. 8 Two-point velocity correlation $R_{uu}(\xi, y)$: (**a**) Ma = 0.8, Re_τ = 7,300 for different wall heights y/δ (■ = 0.15; ∘ = 0.2; ∗ = 0.3; ♦ = 0.5; ◁ = 0.7; × = 1.0). (**b**) Reynolds numbers scaling at $y/\delta = 0.2$ (■, Re_τ = 5,100 (Ma = 0.5); ∘, Re_τ = 9,500 (Ma = 0.5); ∗, Re_τ = 7,800 (Ma = 0.8))

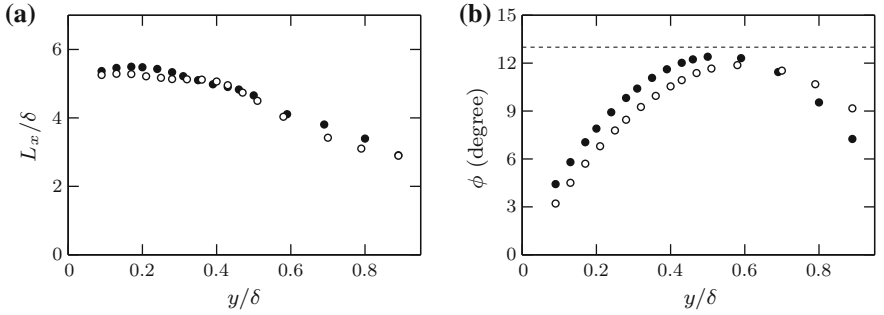

Fig. 9 Streamwise length-scale (**a**) and inclination angle (**b**) of the coherent large-scale structures for different wall heights y/δ: •, Re_τ = 5,100 (Ma = 0.5); ∘, Re_τ = 7,300 (Ma = 0.8)

5 Space-Time PressureVelocity Correlations

Possible links between the large-scale flow structures and wall pressure fluctuations are assessed by means of the space-time correlation R_{pu} defined as:

$$R_{pu}(x, y, \tau) = \langle\, p(x_0, 0, t-\tau)\, u(x, y, t)\,\rangle \,/\, (\rho\, u_\tau^3), \tag{3}$$

where $(x_0, 0)$ is the position of the transducer $\mathcal{P}5$, t the time of the velocity field recording and $\langle\,\rangle$ the ensemble average over all velocity field realisations. Additionally, the space-time correlation is conditioned on the occurrence of positive and negative pressure fluctuation to obtain $R_{pu\,|\,p>0}$ and $R_{pu\,|\,p<0}$.

Figure 10a shows the space-time correlation $R_{pu}(x, y, 0)$ for Re_τ = 5,100 (Ma = 0.5). Positive correlations exists upstream of the reference point, while a large region (4–5 δ) of negative correlation extends downstream of the reference

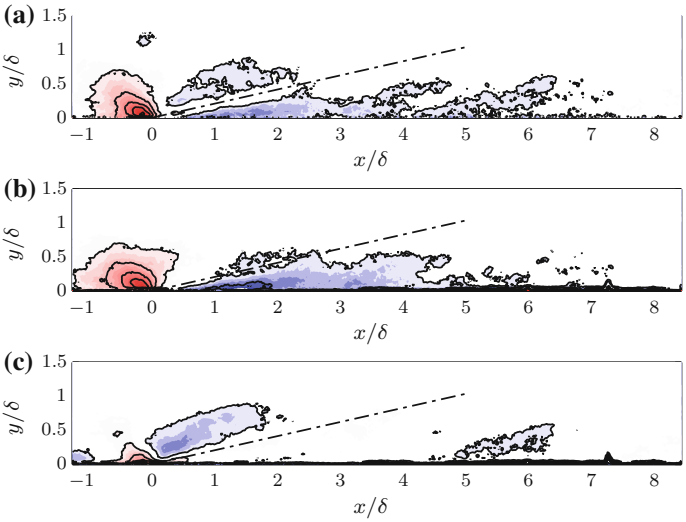

Fig. 10 Space-time correlations $R_{pu}(x, y, 0)$ at $\mathrm{Re}_\tau = 5{,}100$ (Ma = 0.5): (**a**) R_{pu}; (**b**) $R_{pu\,|\,p>0}$; (**c**) $R_{pu\,|\,p<0}$. The *dashed line* indicates an inclination angle of 12°. Contour levels are $R_{pu}/(\rho u_\tau^3) = -20$ to 75 in intervals of 15

point. According to Thomas and Bull [13], wall pressure fluctuations are associated with sweep−ejection events and the formation of the inclined shear layer upstream of the coherent structures. Indeed the negative pressure velocity fluctuations show an inclination angle of approximately 12°, which is consistent with the inclination of the coherent large-scale structures. Additionally, the conditioned space-time correlations reveal a strong link between the large-scale shear layer structures and positive pressure fluctuations (Fig. 10b). On the other hand, negative pressure fluctuations only exhibit a weak link with the large-scale streamwise flow organisation. The significant streamwise (6–7 δ) and wall-normal (0.75 δ) extend of the pressure-velocity correlation R_{pu} and $R_{pu\,|\,p>0}$ suggest that large-scale flow structures play an important role in determining the near wall velocity and wall pressure field.

6 Concluding Remarks

Relationships between large-scale streamwise velocity fluctuations and wall pressure fluctuations in a turbulent boundary layer are investigated. Velocity and pressure statistics at Ma = 0.5–0.8, $\mathrm{Re}_\tau = 5{,}100$–$9{,}500$ are analysed and compare well with existing low Mach number data. Analysis of the streamwise two-point velocity correlation reveals the size (4–6 δ) and orientation of the large-scale flow structures. When scaled on outer units, two-point correlations, averaged structure length and inclination angle collapse for the current range of Mach and Reynolds numbers.

Space-time correlations between wall pressure and streamwise velocity fluctuations reveal structures of large streamwise extent (5–6 δ). Positive pressure fluctuations are strongly correlated with negative velocity fluctuations, which provides evidence of a possible link between the large-scale flow structures in the buffer and outer layer and the near wall pressure field.

References

1. M.K. Bull, A.S.W. Thomas, High frequency wall pressure fluctuations in a turbulent boundary layer. Phys. Fluids **19**, 597–599 (1976)
2. P.A. Chang, U. Piomelli, W.K. Blake, Relationship between wall pressure and velocity-field sources. Phys. Fluids **11**, 3434–3448 (1999)
3. K. Ehrenfried, L. Koop, Experimental study of pressure fluctuations beneath a compressible turbulent boundary layer. In *29th AIAA Aeroacoustics Conference*, Vancouver, British Columbia Canada (2008)
4. T.M. Farabee, M.J. Casarella, Spectral features of wall pressure fluctuations beneath turbulent boundary layer. Phys. Fluids A **3**, 2419–2420 (1991)
5. H.H. Fernholz, P.J. Finley, The incompressible zero-pressure-gradient turbulent boundary layer: an assessment of the data. Prog. Aerosp. Sci. **32**, 245–311 (1996)
6. S. Ghaemi, F. Scarano, Turbulent structure of high-amplitude pressure peaks within the turbulent boundary layer. J. Fluid Mech. **735**, 381–426 (2013)
7. S.P. Gravante, A.M. Naguib, C.E. Wark, H.M. Nagib, Characterization of the pressure fluctuations under a fully developed turbulent boundary layer. AIAA J. **36**, 1808–1816 (1998)
8. N. Hutchins, I. Marusic, Evidence of very long meandering features in the logarithmic region of turbulent boundary layers. J. Fluid Mech. **579**, 1–28 (2007)
9. R. Mathis, N. Hutchins, I. Marusic, Large-scale amplitude modulation of the small-scale structures in turbulent boundary layers. J. Fluid Mech. **628**, 311—337 (2009)
10. A.M. Naguib, C.E. Wark, O. Juckenhöfel, Stochastic estimation and flow sources associated with surface pressure events in a turbulent boundary layer. Phys. Fluids **13**, 2611–2626 (2001)
11. G. Schewe, On the structure and resolution of wall-pressure fluctuations associated with turbulent boundary-layer flow. J. Fluid Mech. **134**, 311–328 (1983)
12. P.R. Spalart, Direct simulation if a turbulent boundary layer up to $R_\theta = 1410$. J. Fluid Mech. **187**, 61–98 (1988)
13. A.S.W. Thomas, M.K. Bull, On the role of wall-pressure fluctuations in deterministic motion in the turbulent boundary layer. J. Fluids Eng. **128**, 283–322 (1983)
14. Y. Tsuji, J.H.M. Fransson, P.H. Alfredsson, A.V. Johansson, Pressure statistics and their scaling in high-Reynolds-number turbulent boundary layers. J. Fluid Mech. **585**, 1–40 (2007)